Received: 10 May 2019 | Revised: 28 December 2019 | Accepted: 6 February 2020

DOI: 10.4218/etrij.2019-0253

ORIGINAL ARTICLE

ETRI Journal WILEY

Fast-convergence trilinear decomposition algorithm for angle and range estimation in FDA-MIMO radar

Cheng Wang | **Wang Zheng** | **Jianfeng Li** | **Pan Gong** | **Zheng Li**

College of Electronic and Information Engineering, Nanjing University of Aeronautics and Astronautics; Key Laboratory of Dynamic Cognitive System of Electromagnetic Spectrum Space (Nanjing University of Aeronautics and Astronautics), Ministry of Industry and Information Technology, Nanjing, 211106, China

Correspondence
Cheng Wang, College of Electronic and Information Engineering, Nanjing University of Aeronautics and Astronautics; Key Laboratory of Dynamic Cognitive System of Electromagnetic Spectrum Space (Nanjing University of Aeronautics and Astronautics), Ministry of Industry and Information Technology, No. 29, Jiangjun Road, Nanjing, Jiangsu Province 211106, China.
Email: chengw@nuaa.edu.cn

Funding information
National Natural Science Foundation of China, Grant/Award Number:61601167, 61971217, 61631020; The fund of Sonar technology key laboratory (Research on the theory and algorithm of signal processing for two-dimensional underwater acoustics coprime array, Range estimation and location technology of passive target via multiple array combination); Fundamental Research Funds for the Central Universities, Grant/Award Number: NT2019013

A frequency diverse array (FDA) multiple-input multiple-output (MIMO) radar employs a small frequency increment across transmit elements to produce an angle-range-dependent beampattern for target angle and range detection. The joint angle and range estimation problem is a trilinear model. The traditional trilinear alternating least square (TALS) algorithm involves high computational load due to excessive iterations. We propose a fast-convergence trilinear decomposition (FC-TD) algorithm to jointly estimate FDA-MIMO radar target angle and range. We first use a propagator method to obtain coarse angle and range estimates in the data domain. Next, the coarse estimates are used as initialized parameters instead of the traditional TALS algorithm random initialization to reduce iterations and accelerate convergence. Finally, fine angle and range estimates are derived and automatically paired. Compared to the traditional TALS algorithm, the proposed FC-TD algorithm has lower computational complexity with no estimation performance degradation. Moreover, Cramér-Rao bounds are presented and simulation results are provided to validate the proposed FC-TD algorithm effectiveness.

KEYWORDS
fast convergence, FDA-MIMO radar, joint angle and range estimation, propagator method, trilinear decomposition

1 | INTRODUCTION

Unlike the traditional phased-array radar, the multiple-input multiple-output (MIMO) radar transmits multiple orthogonal waveforms by multiple elements and receives multiple return echoes by multiple elements, leading to remarkable enhancement in the degrees of freedom (DOFs) and system capacity [1–4]. In application, many direction of arrival estimation algorithms, such as maximal likelihood (ML) [5], multiple signal classification (MUSIC) [6], and Capon algorithm, [7–9] have been investigated. The target angles are obtained by the estimation of signal parameters by the rotational invariance technique (ESPRIT) algorithm [10]. The propagator

method (PM) divides the steering matrix into two submatrices $\mathbf{A}_1$ and $\mathbf{A}_2$, and utilizes the propagation properties of $\mathbf{A}_1$ and $\mathbf{A}_2$ to construct propagator $\mathbf{P}_c$, that is, $\mathbf{A}_2 = \mathbf{P}_c^H \mathbf{A}_1$, to obtain angle and range information, which avoids eigenvalue decomposition (EVD) and exhibits low complexity [11]. The trilinear alternating least square (TALS) algorithm [12] can be effectively employed to resolve the problem of multiple target detection. Multiparameter estimation is also involved in MIMO radar. Two-dimensional (2D) angle estimation is conducted by a variant of the propagator algorithm [13]. The joint Doppler frequency and angle estimation is investigated [2,14], where the compressed sensing and parallel factor algorithms are employed. However, the range parameter has not been involved.

Fortunately, the frequency diverse array (FDA) can locate targets in the joint angle-range dimension by employing a small frequency increment across the array elements to provide additional DOFs of range, which has been utilized in interference detection, joint angle-range beamforming, and spatial filtering. The FDA-MIMO radar coordinates FDA and MIMO radar to produce an angle-range-dependent beampattern [15], which consists of FDA in the transmit and phased arrays in the receive array. As the FDA-MIMO radar possesses various advantages, such as estimating the angle and range of target, improving moving target detection performance, and mitigation of the space-range sidelobe, it has received considerable attention and many joint angle and range estimation algorithms have been proposed. An improved algorithm that utilizes the rotational invariance property, namely the successive ESPRIT algorithm [16], is proposed, and the angles, ranges, and polarization parameters of targets are sequentially estimated. The transmit sub-aperture optimization method [17] is proposed with convex optimization, whereas 2D spectrum peak search (SPS) is involved and hence brings a heavy computational load. The reduced-dimension -MUSIC algorithm [18] is conducted to reduce the computational complexity, but the one-dimensional (1D) SPS is required. A high-accuracy estimation scheme [19] with high computational load is proposed in the FDA-MIMO radar, which exploits the range dependence compensation technique and ML algorithm.

This paper proposes a fast-convergence trilinear decomposition (FC-TD) algorithm for the monostatic FDA-MIMO radar that aims to indicate targets in terms of angle and range with low complexity. The monostatic FDA-MIMO radar is configured with transmit uniform linear array (ULA) and receive ULA. Specifically, the received signal is constructed as a trilinear model and the traditional TALS algorithm is employed. To reduce iteration times and accelerate convergence, the coarse estimates generated by PM are utilized instead of the random initialization of the traditional TALS algorithm. Subsequently, the fine estimates of the angle and range are obtained and automatically paired. Compared with the traditional TALS algorithm, the computational complexity of the proposed FC-TD algorithm is remarkably reduced with no estimation performance degradation. Moreover, the proposed FC-TD algorithm outperforms PM and ESPRIT algorithms in terms of estimation accuracy. Additionally, Cramér-Rao bounds (CRBs) are provided and the effectiveness of the proposed FC-TD algorithm is verified by numerical simulations.

The contributions of this study can be concluded as follows:

1. We formulate the problem of angle-range indication of targets in the FDA-MIMO radar as a trilinear model.
2. We employ coarse estimates generated by PM instead of random initialization to reduce the iteration times of the traditional TALS algorithm, resulting in faster convergence speed and lower computational complexity with no performance degradation.
3. We perform the proposed FC-TD algorithm in the data domain to detect targets, and the angle and range estimates are automatically paired.

The remainder of this paper is summarized as follows: The signal model of the FDA-MIMO radar is formulated in Section 2. In Section 3, the proposed FC-TD algorithm is investigated. Next, we describe the analysis complexity, advantages, and CRBs in Section 4. In Section 5, the simulation results are presented. Finally, the conclusion is presented in Section 6.

Notation: Lower-case (upper-case) bold characters represent vectors (matrices). $(.)^T$, $(.)^*$, $(.)^H$, $(.)^{-1}$, $(.)^{+1}$ are defined as the transpose, conjugate, conjugate-transpose, inverse transformation, and pseudo inverse transformation. $\oplus$, $\otimes$, and $\odot$ represent the Hadamard product, Kronecker product, and Khatri-Rao product. *diag*(.) and $\|.\|_F$ are to construct a diagonal matrix and calculate Frobenius norm. *angle*{.} and *normal*{.} are used to extract the phase angle of the complex value and normalize the vector.

2 | DATA MODEL

2.1 | FDA-MIMO model

The framework of the monostatic FDA-MIMO is shown in Figure 1, where the transmit array consists of N elements and the receive array is composed of M elements. Both transmit and receive arrays are ULAs. The carrier frequency of the n-th transmit element is given as [19],

$$f_n = f_1 + (n-1)\Delta f, \quad n = 1,2, \ldots, N, \tag{1}$$

where f_1 is the reference frequency, Δf stands for the frequency increment across the transmit elements, and $\Delta f \ll f_1$ [20]. To obtain a unique estimate, the transmit array interspace d_T and receive array interspace d_R are set to half wavelength with respect to the carrier wave of the N-th transmit element, that is,

$$d_T = d_R = c/2f_N = c/2(f_1 + (N-1)\Delta f), \tag{2}$$

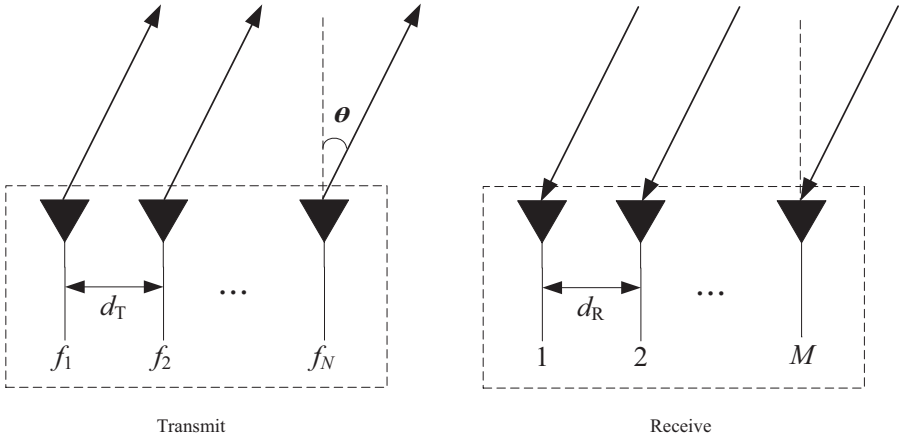

FIGURE 1 Framework of monostatic FDA-MIMO radar

where c is the speed of light.

The n-th transmitted signal of the FDA-MIMO radar can be presented as [19]:

$$\tilde{s}_n(t)=\sqrt{\frac{E}{N}}\varphi_n(t)e^{j2\pi f_n t},\quad 0\le t\le T,\quad n=1,2,\ldots,N, \tag{3}$$

where T is the pulse duration, E is the total transmitted energy, and $\varphi_n(t)$ is defined as the unity-energy wave form which satisfies the orthogonality constraint, that is [19],

$$\int_0^T \varphi_{n_1}(t)\varphi_{n_2}(t-\tau)e^{j2\pi\Delta f(n_1-n_2)t}dt=\begin{cases}0, n_1\neq n_2, \forall\tau,\\ 1, n_1=n_2, \tau=0,\end{cases} \tag{4}$$

where τ is the time delay. Defining the first receive element as the reference point and assuming that the electromagnetic waves are transmitted independently in the scenario with non-cooperative targets, the reflected wave received by the m-th receive element is expressed as [19]:

$$y_m(t)=\sum_{n=1}^{N}\sqrt{\frac{E}{N}}\xi\varphi_n(t-\tau_{n,\mathrm{T}}-\tau_{m,\mathrm{R}})e^{j2\pi(f_n+f_{d,n})(t-\tau_{n,\mathrm{T}}-\tau_{m,\mathrm{R}})}, \tag{5}$$

where ξ denotes radar cross section and $f_{d,n}$ is the Doppler frequency. Additionally, $\tau_{n,\mathrm{T}}$ and $\tau_{m,\mathrm{R}}$ represent the transmit and receive time delay, respectively, which are constructed as,

$$\tau_{n,\mathrm{T}}=\frac{1}{c}[r-d_{\mathrm{T}}(n-1)\sin(\theta)]=\frac{\tau_0}{2}-\frac{d_{\mathrm{T}}}{c}(n-1)\sin(\theta), \tag{6a}$$

$$\tau_{\mathrm{m,R}}=\frac{1}{c}[r-d_{\mathrm{R}}(m-1)\sin(\theta)]=\frac{\tau_0}{2}-\frac{d_{\mathrm{R}}}{c}(m-1)\sin(\theta), \tag{6b}$$

where $\tau_0=2r/c$, θ, and r denote the angle and range of target. Subsequently, in the noise-free case, the received signal will be matched filtered and the n-th output of the m-th receive element is represented by [19]

$$\begin{aligned}&y_{mn}(t)\\&=\sqrt{\frac{E}{N}}\xi e^{j2\pi f_d(t-\tau_0)}e^{-j2\pi\frac{f_n}{c}2r}e^{j2\pi\frac{f_n+f_d}{c}[d_{\mathrm{T}}(n-1)\sin(\theta)+d_{\mathrm{R}}(m-1)\sin(\theta)]}\\&\approx\sqrt{\frac{E}{N}}\xi e^{j2\pi f_d(t-\tau_0)}e^{-j4\pi\frac{f_1}{c}r}e^{-j4\pi\frac{\Delta f}{c}(n-1)r}e^{j2\pi\frac{f_1}{c}[d_{\mathrm{T}}(n-1)\sin(\theta)+d_{\mathrm{R}}(m-1)\sin(\theta)]}\end{aligned} \tag{7}$$

where $f_d \ll f_1$ and $\Delta f \ll f_1$.

2.2 | Single target

According to (7), the output of the m-th receive element can be further formulated as,

$$\mathbf{y}_m(t)=e^{j2\pi\frac{d_R}{\lambda_0}(m-1)\sin(\theta)}\begin{bmatrix}1\\ e^{-j4\pi\frac{\Delta f}{c}r+j2\pi\frac{d_{\mathrm{T}}}{\lambda_0}\sin(\theta)}\\ \vdots\\ e^{-j4\pi\frac{\Delta f}{c}(N-1)r+j2\pi\frac{d_{\mathrm{T}}}{\lambda_0}(N-1)\sin(\theta)}\end{bmatrix}s(t), \tag{8}$$

where $\boldsymbol{y}_m(t)\in\mathbb{C}^{N\times 1}$, $s(t)=\sqrt{E/N}\xi\, e^{j2\pi f_d(t-\tau_0)}e^{-j4\pi f_1 r/c}$, and $\boldsymbol{n}_m(t)\in\mathbb{C}^{N\times 1}$ is the received noise vector. For all the receive elements, the total vectorization output can be presented by [19]

$$\mathbf{x}_s(t)=[\mathbf{y}_1^{\mathrm{T}}(t),\ \mathbf{y}_2^{\mathrm{T}}(t),\ \ldots,\ \mathbf{y}_M^{\mathrm{T}}(t)]^{\mathrm{T}}=[\mathbf{a}_r(\theta)\otimes\mathbf{a}_t(r,\theta)]s(t), \tag{9}$$

where $\mathbf{a}_t(r,\theta)\in\mathbb{C}^{N\times 1}$ and $\mathbf{a}_r(\theta)\in\mathbb{C}^{M\times 1}$ are the transmit and receive steering vectors [21], that is,

$$\mathbf{a}_t(r,\theta)=\begin{bmatrix}1\\ e^{-j4\pi\frac{\Delta f}{c}r+j2\pi\frac{d_{\mathrm{T}}}{\lambda_0}\sin(\theta)}\\ \vdots\\ e^{-j4\pi\frac{\Delta f}{c}(N-1)r+j2\pi\frac{d_{\mathrm{T}}}{\lambda_0}(N-1)\sin(\theta)}\end{bmatrix}=\mathbf{r}(r)\oplus\mathbf{d}(\theta), \tag{10}$$

$$\mathbf{a}_r(\theta)=\left[1, e^{j2\pi d_{\mathrm{R}}\sin(\theta)/\lambda_0},\ \ldots,\ e^{j2\pi d_{\mathrm{R}}(M-1)\sin(\theta)/\lambda_0}\right]^{\mathrm{T}}, \tag{11}$$

where $\oplus$ is the Hadamard product. The transmit range steering vector and transmit angle steering vector are defined as [19],

$$\mathbf{r}(r)=\left[1,\ e^{-j4\pi\Delta fr/c},\ \ldots,\ e^{-j4\pi\Delta f(N-1)r/c}\right]^{\mathrm{T}}, \tag{12}$$

$$\mathbf{d}(\theta)=\left[1,\ e^{j2\pi d_{\mathrm{T}}\sin(\theta)/\lambda_0},\ \ldots,\ e^{j2\pi d_{\mathrm{T}}(N-1)\sin(\theta)/\lambda_0}\right]^{\mathrm{T}}. \tag{13}$$

As shown in (12), the FDA-MIMO radar will be the same as the traditional MIMO radar if $\Delta f=0$.

2.3 | Multiple targets

In the noise case, we assume that there are K independent targets with range and angle (r_k, θ_k), $k=1, 2, \ldots, K$ in the far-field. The output in (9) can be reconstructed as

$$\mathbf{X}=\left[\mathbf{A}_r\odot\mathbf{A}_t\right]\mathbf{S}+\mathbf{N}=\mathbf{AS}+\mathbf{N}, \tag{14}$$

where $\mathbf{A}_t=[\mathbf{a}_t(r_1,\theta_1), \mathbf{a}_t(r_2,\theta_2),\ldots, \mathbf{a}_t(r_K,\theta_K)]$, $\mathbf{A}_r=[\mathbf{a}_r(\theta_1), \mathbf{a}_r(\theta_2), \ldots, \mathbf{a}_r(\theta_K)]$, $\mathbf{S}=[\mathbf{s}(1),\mathbf{s}(2),\ldots,\mathbf{s}(L)]\in\mathbb{C}^{K\times L}$ is the signal matrix and $\mathbf{N}=[\mathbf{n}(1),\mathbf{n}(2),\ldots,\mathbf{n}(L)]\in\mathbb{C}^{MN\times L}$ represents the noise matrix. In addition, $\mathbf{A}=\mathbf{A}_r\odot\mathbf{A}_t$, L is the number of snapshots, $\odot$ represents the Khatri-Rao product, $\mathbf{n}(l)$ is the white circularly Gaussian noise vector with mean zero and variance σ^2 [22], which is independent of signals, and the signal vector $\mathbf{s}(l)$ is given by,

$$\mathbf{s}(l)=\left[s_1(l), s_2(l),\ \ldots, s_K(l)\right]^{\mathrm{T}}=\sqrt{\frac{E}{N}}\begin{bmatrix}\xi_1\, e^{j2\pi f_{d_1}(l-\tau_0)}e^{-j4\pi f_0 r_1/c}\\ \xi_2\, e^{j2\pi f_{d_2}(l-\tau_0)}e^{-j4\pi f_0 r_2/c}\\ \vdots\\ \xi_K\, e^{j2\pi f_{d_K}(l-\tau_0)}e^{-j4\pi f_0 r_K/c}\end{bmatrix}.$$

3 | PROPOSED ALGORITHM

3.1 | Trilinear model

As shown in (14), we can partition $\mathbf{X}$ as [23],

$$\mathbf{X}=\begin{bmatrix}\mathbf{X}_1\\ \mathbf{X}_2\\ \vdots\\ \mathbf{X}_M\end{bmatrix}=\begin{bmatrix}\mathbf{A}_tD_1(\mathbf{A}_r)\\ \mathbf{A}_tD_2(\mathbf{A}_r)\\ \vdots\\ \mathbf{A}_tD_M(\mathbf{A}_r)\end{bmatrix}\mathbf{S}+\begin{bmatrix}\mathbf{N}_1\\ \mathbf{N}_2\\ \vdots\\ \mathbf{N}_M\end{bmatrix}, \tag{15}$$

where $D_m(\mathbf{A}_r)$ is a diagonal matrix consisting of the m-th row of $\mathbf{A}_r$, $\mathbf{X}_m$ is denoted as [24],

$$\mathbf{X}_m=\mathbf{A}_tD_m(\mathbf{A}_r)\mathbf{S}+\mathbf{N}_m,\ m=1,\ 2,\ \ldots,\ M. \tag{16}$$

In the noise-free case, the (n, l) element of $\mathbf{X}_m$ can be constructed as [25,26],

$$x(n,m,l)=\sum_{k=1}^{K}\mathbf{A}_t(n,k)\mathbf{A}_r(m,k)\mathbf{S}(k,l)$$
$$n=1,2,\ldots,N,\ m=1,2,\ldots,M,\ l=1,2,\ldots,L, \tag{17}$$

where $\mathbf{A}_t(n, k)$ denotes the (n, k) element of $\mathbf{A}_t$ and similarly for the others. As shown in (17), the arbitrary element in $\mathbf{X}$ can be expressed as a trilinear model which is shown in Figures 2, and $\mathbf{X}$ can be rearranged as two different matrices $\mathbf{Y}$ and $\mathbf{Z}$, that is,

$$\mathbf{Y}=\begin{bmatrix}\mathbf{Y}_1\\ \mathbf{Y}_2\\ \vdots\\ \mathbf{Y}_L\end{bmatrix}=\begin{bmatrix}\mathbf{A}_rD_1\left(\mathbf{S}^T\right)\\ \mathbf{A}_rD_2\left(\mathbf{S}^{\mathrm{T}}\right)\\ \vdots\\ \mathbf{A}_rD_L\left(\mathbf{S}^{\mathrm{T}}\right)\end{bmatrix}\mathbf{A}_t^{\mathrm{T}}+\begin{bmatrix}\mathbf{N}_1\\ \mathbf{N}_2\\ \vdots\\ \mathbf{N}_L\end{bmatrix}=\left[\mathbf{S}^{\mathrm{T}}\odot\mathbf{A}_r\right]\mathbf{A}_t^{\mathrm{T}}+\begin{bmatrix}\mathbf{N}_1\\ \mathbf{N}_2\\ \vdots\\ \mathbf{N}_L\end{bmatrix}, \tag{18}$$

$$\begin{aligned}\mathbf{Z}&=\begin{bmatrix}\mathbf{Z}_1\\ \mathbf{Z}_2\\ \vdots\\ \mathbf{Z}_N\end{bmatrix}=\begin{bmatrix}\mathbf{S}^{\mathrm{T}}D_1\left(\mathbf{A}_t\right)\\ \mathbf{S}^{\mathrm{T}}D_2\left(\mathbf{A}_t\right)\\ \vdots\\ \mathbf{S}^{\mathrm{T}}D_N\left(\mathbf{A}_t\right)\end{bmatrix}\mathbf{A}_r^{\mathrm{T}}+\begin{bmatrix}\mathbf{N}_1\\ \mathbf{N}_2\\ \vdots\\ \mathbf{N}_N\end{bmatrix}\\ &=\left[\mathbf{A}_t\odot\mathbf{S}^{\mathrm{T}}\right]\mathbf{A}_r^{\mathrm{T}}+\begin{bmatrix}\mathbf{N}_1\\ \mathbf{N}_2\\ \vdots\\ \mathbf{N}_N\end{bmatrix}.\end{aligned} \tag{19}$$

In the traditional TALS algorithm, the random initialization results in many iterations and a heavy computational load. To improve computation efficiency, the coarse estimates generated by PM are employed for initialization instead of random initialization estimates, which remarkably reduces the iteration times and accelerates convergence.

3.2 | Initializing with PM

Assuming that the first K rows of steering matrix $\mathbf{A}$ are linearly independent, we can partition $\mathbf{A}$ as

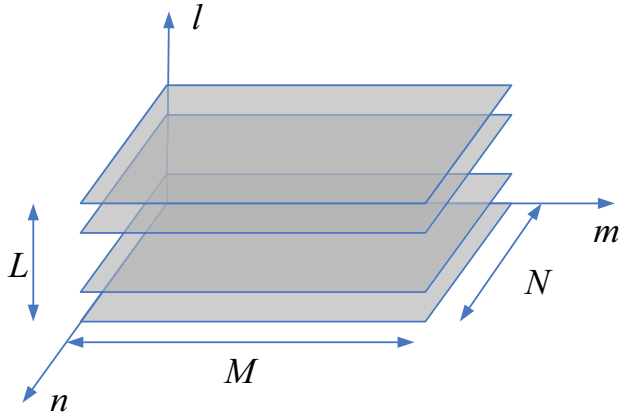

FIGURE 2 Trilinear model

$$\mathbf{A}=\begin{bmatrix}\mathbf{A}_1\\ \mathbf{A}_2\end{bmatrix}, \tag{20}$$

where $\boldsymbol{A}_1\in\mathbb{C}^{K\times K}$ is assumed to be a nonsingular matrix and $\boldsymbol{A}_2\in\mathbb{C}^{(MN-K)\times K}$. Specifically, $\mathbf{A}_2$ can be linearly expressed by $\mathbf{A}_1$ [27], that is,

$$\mathbf{A}_2=\mathbf{P}_{\mathrm{c}}^{\mathrm{H}}\mathbf{A}_1, \tag{21}$$

where $\boldsymbol{P}_{\mathrm{c}}\in\mathbb{C}^{K\times(MN-K)}$ is a propagator matrix. In the noise case, the propagator matrix is calculated as [28]

$$\hat{\mathbf{P}}_{\mathrm{c}}=(\mathbf{X}_1\mathbf{X}_1^{\mathrm{H}})^{-1}\mathbf{X}_1\mathbf{X}_2^{\mathrm{H}}, \tag{22}$$

where $\mathbf{X}_1$ and $\mathbf{X}_2$ are the first K rows and remaining rows of $\mathbf{X}$, respectively. Construct matrix $\mathbf{P}$ as

$$\mathbf{P}=\begin{bmatrix}\mathbf{I}_K\\ \hat{\mathbf{P}}_{\mathrm{c}}^{\mathrm{H}}\end{bmatrix}. \tag{23}$$

In the noise-free case, we have

$$\mathbf{P}\mathbf{A}_1=\mathbf{A}, \tag{24}$$

then we can partition $\mathbf{P}$ as,

$$\begin{bmatrix}\mathbf{P}_a\\ \mathbf{P}_b\end{bmatrix}\mathbf{A}_1=\begin{bmatrix}\mathbf{A}_a\\ \mathbf{A}_b\end{bmatrix}=\begin{bmatrix}\mathbf{A}_a\\ \mathbf{A}_a\boldsymbol{\Phi}_\theta\end{bmatrix}, \tag{25}$$

where $\mathbf{P}_a$ and $\mathbf{P}_b$ stand for the first $(M-1)N$ rows and the last $(M-1)N$ rows of $\mathbf{P}$, $\mathbf{A}_a$ and $\mathbf{A}_b$ denote the first $(M-1)N$ rows and the last $(M-1)N$ rows of $\mathbf{A}$, $\boldsymbol{\Phi}_\theta$ is a diagonal matrix which contains $e^{j2\pi d_{\mathrm{T}}\sin(\theta_k)/\lambda_0}$, $k=1, 2, \ldots, K$ in the diagonal elements. Subsequently, we can achieve [29]

$$\mathbf{P}_a^{+}\mathbf{P}_b=\mathbf{A}_1\boldsymbol{\Phi}_\theta\mathbf{A}_1^{-1}. \tag{26}$$

Next, we can get $\hat{\boldsymbol{\Phi}}_\theta$ and $\hat{\mathbf{A}}_1$ by performing EVD on $\mathbf{P}_a^{+}\mathbf{P}_b$. Finally, the coarse angle estimate is expressed as

$$\hat{\theta}_{c,k}=\arcsin\left(\frac{angle\left(\hat{\boldsymbol{\Phi}}_\theta^{k}\right)\lambda_0}{2\pi d_R}\right), k=1,2,\ldots,K, \tag{27}$$

where $\hat{\boldsymbol{\Phi}}_\theta^{k}$ is the k-th diagonal element of $\hat{\boldsymbol{\Phi}}_\theta$.

Similarly, the ranges of targets can be estimated by utilizing the rotational invariance property again. To be more specific, the steering matrix in (14) is rearranged as,

$$\mathbf{A}'=\mathbf{J}\mathbf{A}, \tag{28}$$

where $\mathbf{J}\in\mathbb{C}^{MN\times L}$ is an elementary row transformation matrix which is constructed as [25],

$$J(i,j)=\begin{cases}1, i=(n-1)M+m+1, j=mN+n\ n=1,\ 2,\ \ldots,\ N,\\ 0, \text{ else } m=0,\ 1,\ \ldots,\ M-1.\end{cases} \tag{29}$$

According to (24) and (28), we can have,

$$\mathbf{J}\mathbf{P}\mathbf{A}_1=\mathbf{P}'\mathbf{A}_1=\mathbf{A}', \tag{30}$$

where $\mathbf{P}'=\mathbf{J}\mathbf{P}$, then we can achieve,

$$\begin{bmatrix}\mathbf{P}'_a\\ \mathbf{P}'_b\end{bmatrix}\mathbf{A}_1=\begin{bmatrix}\mathbf{A}'_a\\ \mathbf{A}'_b\end{bmatrix}=\begin{bmatrix}\mathbf{A}'_a\\ \mathbf{A}'_a\boldsymbol{\Phi}_{r,\theta}\end{bmatrix}, \tag{31}$$

where $\mathbf{P}'_a$ and $\mathbf{P}'_b$ represent the first $(N-1)M$ rows and the last $(N-1)M$ rows of $\mathbf{P}'$; $\mathbf{A}'_a$ and $\mathbf{A}'_b$ denote the first $(N-1)M$ rows and the last $(N-1)M$ rows of $\mathbf{A}'$; $\boldsymbol{\Phi}_{r,\theta}$ is a diagonal matrix which contains $e^{-j4\pi r_k\Delta f/c+j2\pi d_{\mathrm{R}}\sin(\theta_k)/\lambda_0}$; and $k=1, 2, \ldots, K$ in the diagonal elements. Next, the $\boldsymbol{\Phi}_{r,\theta}$ can be estimated as.

$$\hat{\boldsymbol{\Phi}}_{r,\theta}=\hat{\mathbf{A}}_1^{-1}\mathbf{P}'^{+}_a\mathbf{P}'_b\hat{\mathbf{A}}_1, \tag{32}$$

where $\hat{\mathbf{A}}_1$ is utilized to make $\hat{\boldsymbol{\Phi}}_\theta$ and $\hat{\boldsymbol{\Phi}}_{r,\theta}$ have the same permutation ambiguity, which means that the coarse angle estimates and coarse range estimates can be automatically paired. Next, we can have.

$$\hat{\boldsymbol{\Phi}}_r=\hat{\boldsymbol{\Phi}}_{r,\theta}\hat{\boldsymbol{\Phi}}_{c,\theta}, \tag{33}$$

where $\hat{\boldsymbol{\Phi}}_{c,\theta}$ stands for a diagonal matrix which contains $e^{-j2\pi d_{\mathrm{T}}\sin(\hat{\theta}_{c,k})/\lambda_0}$, $k=1, 2, \ldots, K$ in the diagonal elements. Finally, the coarse range estimate is represented as.

$$\hat{r}_{c,k}=\arcsin\left(-\frac{angle\left(\hat{\boldsymbol{\Phi}}_r^{k}\right)c}{4\pi\Delta f}\right), \quad k=1,\ 2,\ \ldots,\ K, \tag{34}$$

where $\hat{\boldsymbol{\Phi}}_r^{k}$ is the k-th diagonal element of $\hat{\boldsymbol{\Phi}}_r$.

3.3 | Trilinear decomposition

The traditional TALS algorithm [30] is employed to decompose the trilinear model, and the coarse estimates are utilized to accelerate convergence.

The major steps are given below. Perform least square (LS) fitting to $\mathbf{X}$, that is,

$$\min_{\mathbf{A}_r,\mathbf{A}_t,\mathbf{S}} \left\| \mathbf{X} - \left(\mathbf{A}_r \odot \mathbf{A}_t \right) \mathbf{S} \right\|_F^2. \tag{35}$$

Then the LS update for $\mathbf{S}$ is [30]

$$\hat{\mathbf{S}} = \left(\hat{\mathbf{A}}_r \odot \hat{\mathbf{A}}_t \right) + \mathbf{X}, \tag{36}$$

where $\hat{\mathbf{A}}_r$ and $\hat{\mathbf{A}}_t$ are the estimates of $\mathbf{A}_r$ and $\mathbf{A}_t$, that are previously obtained but initialized for the first time by (28) and (34), respectively. According to (18), LS fitting is,

$$\min_{\mathbf{A}_r,\mathbf{A}_t,\mathbf{S}} \left\| \mathbf{Y} - \left(\mathbf{S}^{\mathrm{T}} \odot \mathbf{A}_r \right) \mathbf{A}_t^{\mathrm{T}} \right\|_F^2. \tag{37}$$

Next, the LS update for $\mathbf{A}_t$ is,

$$\widehat{\mathbf{A}_t^{\mathrm{T}}} = \left(\hat{\mathbf{S}}^{\mathrm{T}} \odot \hat{\mathbf{A}}_r \right) + \mathbf{Y}, \tag{38}$$

where $\hat{\mathbf{S}}$ and $\hat{\mathbf{A}}_r$ are the estimates of $\mathbf{S}$ and $\mathbf{A}_r$, that are previously obtained. According to (19), LS fitting is,

$$\min_{\mathbf{A}_r,\mathbf{A}_t,\mathbf{S}} \left\| \mathbf{Z} - \left(\mathbf{A}_t \odot \mathbf{S}^{\mathrm{T}} \right) \mathbf{A}_r^{\mathrm{T}} \right\|_F^2. \tag{39}$$

The LS update for $\mathbf{A}_r$ is,

$$\hat{\mathbf{A}}_r^{\mathrm{T}} = \left(\hat{\mathbf{A}}_t \odot \hat{\mathbf{S}}^{\mathrm{T}} \right) + \mathbf{Z}, \tag{40}$$

where $\hat{\mathbf{A}}_t$ and $\hat{\mathbf{S}}$ are the estimates of $\mathbf{A}_t$ and $\mathbf{S}$, that are previously obtained. Denote residuals matrix and the sum of squared residuals (SSR) as [30],

$$C = \mathbf{X} - \left(\hat{\mathbf{A}}_r \odot \hat{\mathbf{A}}_t \right) \hat{\mathbf{S}}, \tag{41}$$

$$\mathrm{SSR} = \sum_{u}^{MN} \sum_{v}^{L} |c_{uv}|^2, \tag{42}$$

respectively, where c_{uv} stands for the (u,v) element of $\mathbf{C}$. According to (36), (38), and (40), the matrix update of $\hat{\mathbf{S}}$, $\hat{\mathbf{A}}_t$, and $\hat{\mathbf{A}}_r$ is repeated until SSR converges and we can get the final estimates $\hat{\mathbf{S}}'$, $\hat{\mathbf{A}}_t'$, and $\hat{\mathbf{A}}_r'$.

Consider the received signal matrix in (15) $\mathbf{X}_m = \mathbf{A}_t D_m(\mathbf{A}_r)\mathbf{S} + \mathbf{N}_m$, $m = 1, 2, \ldots, M$, where $\mathrm{A}_t \in \mathbb{C}^{N\times K}$, $\mathrm{A}_r \in \mathbb{C}^{M\times K}$, and $\mathrm{S}^{\mathrm{T}} \in \mathbb{C}^{L\times K}$. According to the theorem [31], if $\mathbf{A}_t$, $\mathbf{A}_r$, and $\mathbf{S}$ are full k-rank and the parameter identifiability satisfies,

$$k_{\mathbf{A}_t} + k_{\mathbf{A}_r} + k_{\mathbf{S}^{\mathrm{T}}} \geq 2K + 2, \tag{43}$$

then $\hat{\mathbf{A}}_t$, $\hat{\mathbf{A}}_r$, and $\hat{\mathbf{S}}$ will be unique up to permutation and scaling of columns, that is,

$$\hat{\mathbf{A}}_t = \mathbf{A}_t \boldsymbol{\Pi}' \boldsymbol{\eta}_1 + \mathbf{E}_1, \tag{44a}$$

$$\hat{\mathbf{A}}_r = \mathbf{A}_t \boldsymbol{\Pi}' \boldsymbol{\eta}_2 + \mathbf{E}_2, \tag{44b}$$

$$\hat{\mathbf{S}} = \mathbf{S}\boldsymbol{\Pi}' \boldsymbol{\eta}_3 + \mathbf{E}_3, \tag{44c}$$

where $\mathbf{E}_1$, $\mathbf{E}_2$, and $\mathbf{E}_3$ are the estimation error matrices; $\boldsymbol{\eta}_1$, $\boldsymbol{\eta}_2$, and $\boldsymbol{\eta}_3$ are the diagonal scaling matrices satisfying $\boldsymbol{\eta}_1\boldsymbol{\eta}_2\boldsymbol{\eta}_3 = \mathbf{I}_K$; and $\boldsymbol{\Pi}'$ is the permutation matrix.

3.4 | Angle and range estimation

To estimate the target angles, we first normalize the receive steering vectors and extract their phase angle, that is,

$$\hat{\mathbf{g}}_k = angle\left(normal(\hat{\mathbf{a}}_r'(\theta_k))\right), \tag{45}$$

where $\hat{\mathbf{a}}_r'(\theta_k)$ is the k-th column of $\hat{\mathbf{A}}_r'$. Next, perform LS fitting to $\hat{\mathbf{g}}_k$, that is,

$$\min_{\mathbf{c}_k} \left\| \mathbf{G}\mathbf{c}_k - \hat{\mathbf{g}}_k \right\|_F^2, \; k = 1,2,\ldots,K, \tag{46}$$

where $\boldsymbol{c}_k = [c_{k0}, \theta_k]^{\mathrm{T}} \in \mathbb{R}^{2\times 1}$, c_{k0} is parameter error, θ_k is the target angle and,

$$\boldsymbol{G} = \begin{bmatrix} 1 & 0 \\ 1 & 2\pi d_R/\lambda_0 \\ \vdots & \vdots \\ 1 & (M-1)\,2\pi d_R/\lambda_0 \end{bmatrix} \in \mathbb{C}^{M\times 2}.$$

Finally, the K solutions of $\mathbf{c}_k$ are established as,

$$\hat{\mathbf{c}}_k = [\hat{c}_{k0}, \hat{\theta}_k]^{\mathrm{T}} = (\mathbf{G}^{\mathrm{T}}\mathbf{G})^{-1}\mathbf{G}^{\mathrm{T}}\hat{\mathbf{g}}_k, k = 1, 2, \ldots, K, \tag{47}$$

where $\hat{\theta}_k$ is the fine angle estimate. Subsequently, the angle-dependent decomposition vector is formulated to decompose the angle and range information, that is,

$$\mathbf{d}'(\hat{\theta}_k) = [1, e^{-j2\pi d_T \sin\hat{\theta}_k/\lambda_0}, \ldots, e^{-j2\pi(N-1)d_T \sin\hat{\theta}_k/\lambda_0}]^{\mathrm{T}}, \quad k = 1, 2, \ldots, K. \tag{48}$$

Next, the transmit range steering vector is estimated as [32],

$$\hat{\mathbf{r}}(r_k) = \hat{\mathbf{a}}_t'(r_k, \theta_k) \oplus \mathbf{d}'(\hat{\theta}_k), \quad k = 1, 2, \ldots, K, \tag{49}$$

where $\hat{\mathbf{a}}_t'(r_k,\theta_k)$ is the k-th column of $\hat{\mathbf{A}}_t'$ and $\oplus$ is the Hadamard product. Similarly, we normalize the transmit range steering vector and extract their phase angle, that is,

$$\hat{\mathbf{h}}_k = -angle\,(normal(\hat{\mathbf{r}}(r_k))). \tag{50}$$

Perform LS fitting to $\hat{\mathbf{h}}_k$, that is,

$$\min_{\mathbf{p}_k} \left\| \mathbf{H}\mathbf{p}_k - \hat{\mathbf{h}}_k \right\|_F^2, -k = 1, 2, \ldots, K, \tag{51}$$

where $\boldsymbol{p}_k = [p_{k0}, r_k]^{\mathrm{T}} \in \mathbb{R}^{2\times 1}$, p_{k0} is parameter error, r_k is the range of target and,

$$\boldsymbol{H} = \begin{bmatrix} 1 & 0 \\ 1 & 4\pi\Delta f/c \\ \vdots & \vdots \\ 1 & (N-1)\,4\pi\Delta f/c \end{bmatrix} \in \mathbb{C}^{N\times 2}.$$

Finally, the K solutions of $\mathbf{p}_k$ are calculated as,

$$\hat{\mathbf{p}}_k = [\hat{p}_{k0}, \hat{r}_k]^{\mathrm{T}} = (\mathbf{H}^{\mathrm{T}}\mathbf{H})^{-1}\mathbf{H}^{\mathrm{T}}\hat{\mathbf{h}}_k, k = 1, 2, \ldots, K, \tag{52}$$

where $\hat{r}_k$ is the fine range estimate.

The detailed steps of the proposed FC-TD algorithm can be summarized as:

1. Calculate $\hat{\mathbf{P}}_{\mathrm{c}}$ and $\mathbf{P}$ via (22) and (23).
2. Perform EVD to $\mathbf{P}_a^{+}\mathbf{P}_b$ to obtain $\hat{\boldsymbol{\Phi}}_\theta$ and $\hat{\mathbf{A}}_1$ via (26), and calculate $\hat{\theta}_{c,k}$ via (27).
3. Compute $\mathbf{P}' = \mathbf{J}\mathbf{P}$ and $\hat{\boldsymbol{\Phi}}_{r,\theta} = \hat{\mathbf{A}}_1^{-1}\mathbf{P}_a'^{+}\mathbf{P}_b'\hat{\mathbf{A}}_1$ via (32).
4. Calculate $\hat{\boldsymbol{\Phi}}_r = \hat{\boldsymbol{\Phi}}_{r,\theta}\hat{\boldsymbol{\Phi}}_{c,\theta}$ and $\hat{r}_{c,k}$ via (33) and (34).
5. Apply LS fitting to $\mathbf{S}$ via (36).
6. Apply LS fitting to $\mathbf{A}_t$ via (38).
7. Apply LS fitting to $\mathbf{A}_r$ via (40).
8. Repeat step 5 to step 7 until convergence and obtain $\hat{\mathbf{S}}'$, $\hat{\mathbf{A}}_t'$, and $\hat{\mathbf{A}}_r'$.
9. Calculate $\hat{\theta}_k$ and construct $\mathbf{d}'(\hat{\theta}_k)$ via (47) and (48).
10. Formulate $\hat{\mathbf{r}}(r_k)$ and compute $\hat{r}_k$ via (49) and (52).

4 | PERFORMANCE ANALYSIS

4.1 | Complexity analysis

As the random initialization is replaced by the coarse estimates, the proposed FC-TD algorithm has much lower computational load over the traditional TALS algorithm. In the proposed FC-TD algorithm, the complexity of PM is denoted as $O(2K^2L + KL(MN - K) + 7K^2MN - 3K^2(M + N) + 4K^3 + K)$ and the complexity of each iteration of TALS is represented as $O(2K^2(MN + NK + ML)) + MNK + NLK + MLK + 3K^3 + 3KMNL)$. The total complexity of the proposed FC-TD algorithm is defined as $O(2K^2L) + KL(MN - K) + 7K^2MN - 3K^2(M + N) + 4K^3 + K + q_2[(2K^2 + K)(MN + NL + ML) + 3(K^3 + KMNL)] + N)$, where q_2 is the iteration times of the proposed FC-TD algorithm. Specifically, the complexity of the traditional TALS [30], proposed FC-TD, PM [11], and ESPRIT [16] algorithms is listed in Table 1, where q_1 is the iteration times of the traditional TALS algorithm.

According to (42), differential sum of squared residuals (DSSR) is defined as,

$$\mathrm{DSSR} = \mathrm{SSR}_q - \mathrm{SSR}_0, \tag{53}$$

where SSR_q denotes the SSR of the q-th iteration, SSR_0 is the SSR in the convergence case. For better illustration, the iteration times of the traditional TALS and proposed FC-TD algorithm are compared in Figure 3, where $K = 3$ noncoherent targets with $(\theta_1, r_1) = (10°, 200\ \mathrm{m})$, $(\theta_2, r_2) = (20°, 220\ \mathrm{m})$, and $(\theta_3, r_3) = (30°, 240\ \mathrm{m})$ are considered, $\Delta f = 300$ KHz, $f_0 = 10$ GHz, and $SNR = 5$ dB. It is shown that the iteration times of the proposed FC-TD algorithm is much less than that of the traditional

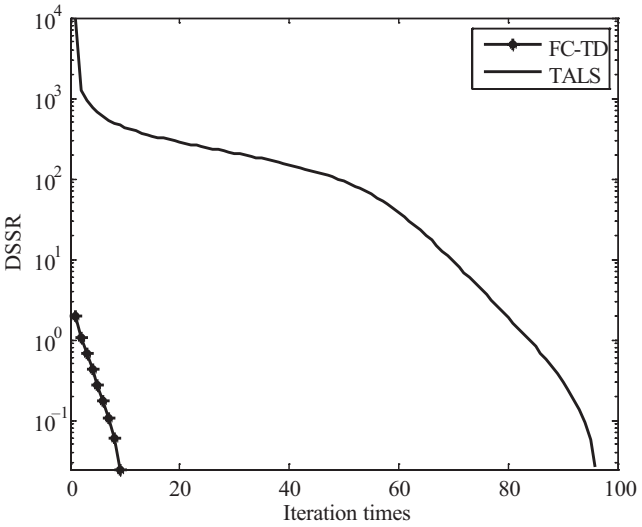

FIGURE 3 Iteration times comparison ($N = 6$, $M = 6$, $L = 400$)

PM	$O(2K^2L + KL(MN - K) + 7K^2MN - 3K^2(M + N) + 4K^3 + K)$
ESPRIT	$O(L(MN)^2 + (MN)^3 + 2K^2(2MN - N - M) + 6K^3)$
TALS	$O(q_1[(2K^2 + K)(MN + NL + ML) + 3(K^3 + KMNL)] + N)$
FC-TD	$O(2K^2L) + KL(MN - K) + 7K^2MN - 3K^2(M + N) + 4K^3 + K + q_2[(2K^2 + K)(MN + NL + ML) + 3(K^3 + KMNL)] + N)$

TABLE 1 Computational complexity comparison

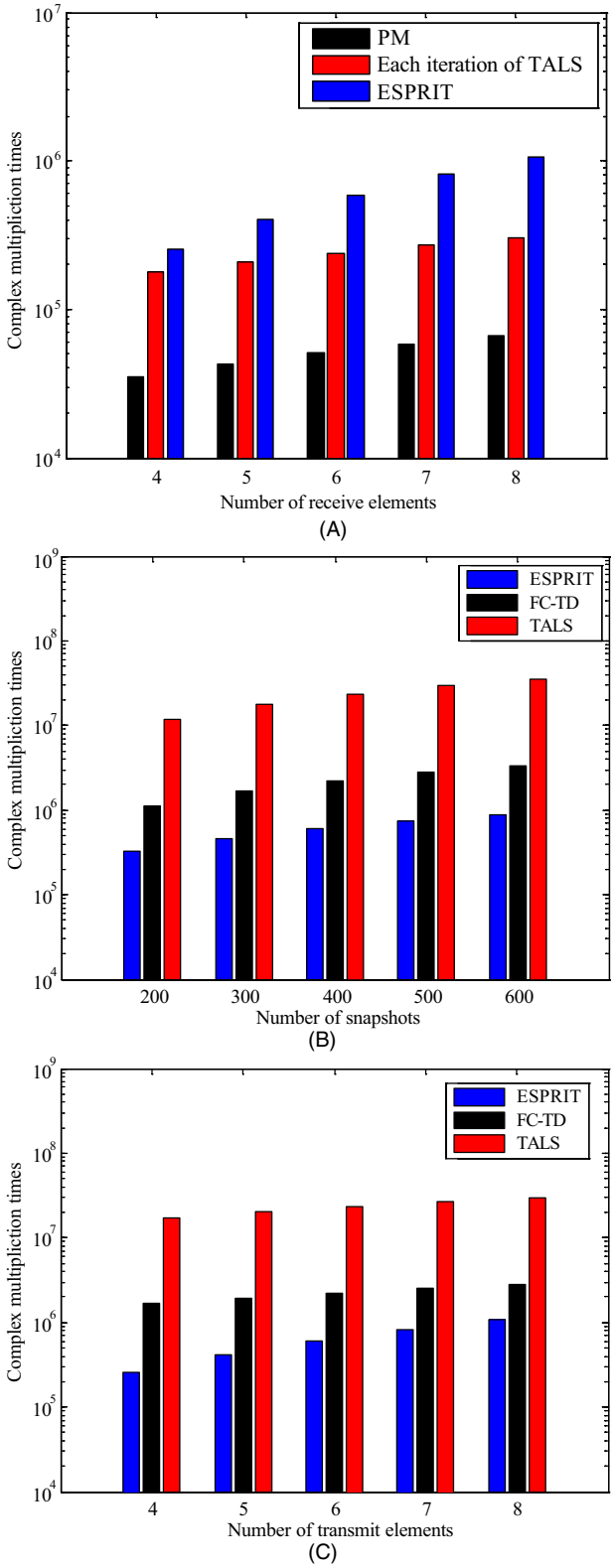

FIGURE 4 (A) Complexity comparison vs receive elements ($N = 6$, $L = 400$). (B) Complexity comparison vs snapshots ($N = 6$, $M = 6$). (C) Complexity comparison vs transmit elements ($M = 6$, $L = 400$)

TALS algorithm, that is, $q_1 = 96$, $q_2 = 9$, which further verifies that the proposed FC-TD algorithm enjoys lower computational complexity.

The complexity comparison of different algorithms is shown in Figure 4, where $K = 3$. Note that the iteration times remain basically unchanged for different array element and snapshot numbers, so we choose $q_1 = 96$, $q_2 = 9$ for all cases in Figure 4. As shown in Figure 4A, we can find that the PM has lower complexity than each iteration of the TALS algorithm, which means that the initialization of PM has little effect on total complexity. Meanwhile, the complexity of PM is much lower than that of the ESPRIT algorithm, which is more suitable for parameter initialization. Figures 4B and 4C depict the complexity comparison of different algorithms vs the number of snapshots and transmit elements. The complexity of the proposed FC-TD algorithm is much lower than that of the traditional TALS algorithm due to fewer iterations.

4.2 | Advantages

We summarize the advantages of the proposed FC-TD algorithm as follows:

1. The proposed FC-TD algorithm has much lower computational complexity than the traditional TALS algorithm due to the utilization of coarse estimates.
2. The proposed FC-TD algorithm outperforms the PM and ESPRIT algorithms and has the same estimation performance compared to the traditional TALS algorithm.
3. The coupling information of angle and range is decomposed, and the angle and range estimates are automatically paired.

Remark 1 The proposed FC-TD algorithm is different from the fast parallel factor decomposition algorithm [30] First, the algorithm [30] is performed in the multiple invariance array, but the proposed FC-TD algorithm is investigated in the FDA-MIMO radar. Second, the algorithm [30] only involves 1D angle estimation problem while the proposed FC-TD algorithm studies the 2D joint angle and range estimation problem. Third, the algorithm [30] utilizes multiple identical ULAs with displacement, but the proposed FC-TD algorithm only employs two ULAs. Thus, the proposed FC-TD algorithm can be regarded as an extension of the algorithm [30].

Remark 2 The proposed FC-TD algorithm is different from the ESPRIT algorithm. First, the ESPRIT algorithm detects the target by performing EVD to the received signal, but the proposed FC-TD algorithm resolves the target localization problem in the data domain. Second, the ESPRIT algorithm can give the closed-form solution of the estimate but the proposed FC-TD algorithm calculates the solution by iteration. Finally, the proposed FC-TD algorithm utilizes the rotational invariance of

multimatrix while ESPRIT uses the rotational invariance of two matrices, thus the proposed FC-TD algorithm can be seen as an extension of ESPRIT.

Remark 3 We assume the source number K is known in this study and if not, we can estimate it by the methods in [33,34].

4.3 | Cramér-Rao Bound

The CRBs of angle and range in the monostatic FDA-MIMO radar are defined as [35],

$$\mathrm{CRB}_{\theta}=\frac{\sigma^2}{2L}\{\mathrm{Re}[(\mathbf{D}_{\theta}^{\mathrm{H}}\boldsymbol{\Pi}_{\mathbf{A}}^{\perp}\mathbf{D}_{\theta})\oplus\mathbf{P}^{\mathrm{T}}]\}^{-1}, \tag{54a}$$

$$\mathrm{CRB}_{\mathrm{r}}=\frac{\sigma^2}{2L}\{\mathrm{Re}[(\mathbf{D}_{\mathrm{r}}^{\mathrm{H}}\boldsymbol{\Pi}_{\mathbf{A}}^{\perp}\mathbf{D}_{\mathrm{r}})\oplus\mathbf{P}^{\mathrm{T}}]\}^{-1}, \tag{54b}$$

where $\mathbf{D}_{\theta}=[\mathbf{d}_{1\theta}\,\mathbf{d}_{2\theta}\,\ldots,\mathbf{d}_{K\theta}]$, $\mathbf{d}_{k\theta}=\partial(\mathbf{b}(\theta_{\mathrm{k}})\otimes\mathbf{a}(r_k,\theta_k))/\partial\theta_k$, $\mathbf{D}_{r}=[\mathbf{d}_{1r},\mathbf{d}_{2r},\ldots,\mathbf{d}_{Kr}]$, and $\mathbf{d}_{kr}=\partial(\mathbf{b}(\theta_k)\otimes\mathbf{a}(r_k,\theta_k))/\partial r_k$. In addition, $\boldsymbol{\Pi}_{\mathbf{A}}^{\perp}=\mathbf{I}_{MN}-\overline{\mathbf{A}}(\overline{\mathbf{A}}^{\mathrm{H}}\overline{\mathbf{A}})^{-1}\overline{\mathbf{A}}^{\mathrm{H}}$ and $\mathbf{P}=(1/L)\sum_{l=1}^{L}\mathbf{s}(l)\mathbf{s}^{\mathrm{H}}(l)$.

5 | SIMULATION RESULTS

In this section, the effectiveness of the proposed FC-TD algorithm is validated by numerical simulations. The root mean square error (RMSE) of angle and range is defined as

$$\mathrm{RMSE}_{\beta}=\frac{1}{K}\sum_{k=1}^{K}\sqrt{\frac{1}{P}\sum_{p=1}^{P}(\hat{\beta}_{k,p}-\beta_k)^2}, \tag{55}$$

where $\hat{\beta}_{k,p}$ is defined as the k-th angle or range estimate of the p-th Monte Carlo trial, β_k denotes the angle or range of k-th target, and P stands for the number of Monte Carlo trials. In all simulations except Figures 8–10, $K=3$ noncoherent targets with $(\theta_1, r_1)=(10°, 200\ \mathrm{m})$, $(\theta_2, r_2)=(20°, 220\ \mathrm{m})$, and $(\theta_3, r_3)=(30°, 240\ \mathrm{m})$ are considered. Unless otherwise stated, all the simulations operating at $f_0=10$ GHz and $\Delta f=300$ KHz.

As shown in Figure 5, the scatter diagram of the joint angle and range estimation result is provided to validate the reliability of the proposed FC-TD algorithm, where $N=6$, $M=8$, $L=200$, and SNR = 5 dB. To this end, we carry out $P=200$ Monte Carlo trials. It is shown that the angles and ranges of targets can be successfully estimated.

For better illustration, the comparison of estimation performance of different algorithms in the FDA-MIMO radar is shown in Figures 6 and 7, where $N=6$ and $M=8$ are

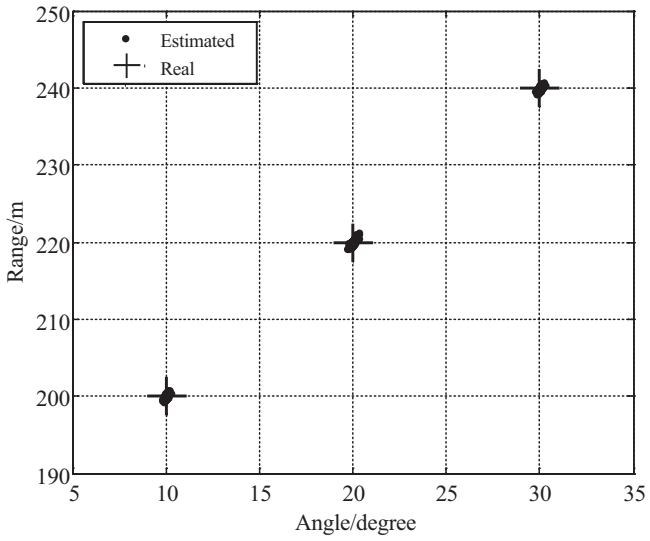

FIGURE 5 Joint angle and range estimation result of proposed FC-TD algorithm ($N=6$, $M=8$, $K=3$, $L=200$, $P=200$, SNR = 5 dB)

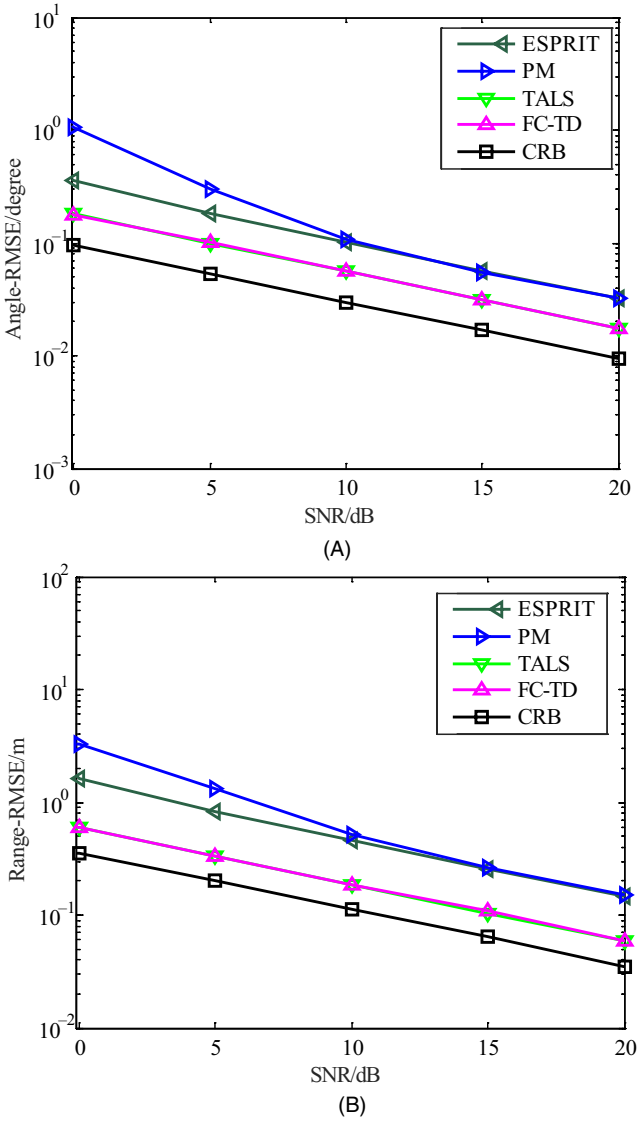

FIGURE 6 (A) Angle RMSE of different algorithms vs SNR, (B) Range RMSE of different algorithms vs SNR ($N=6$, $M=8$, $K=3$, $L=200$, $P=200$)

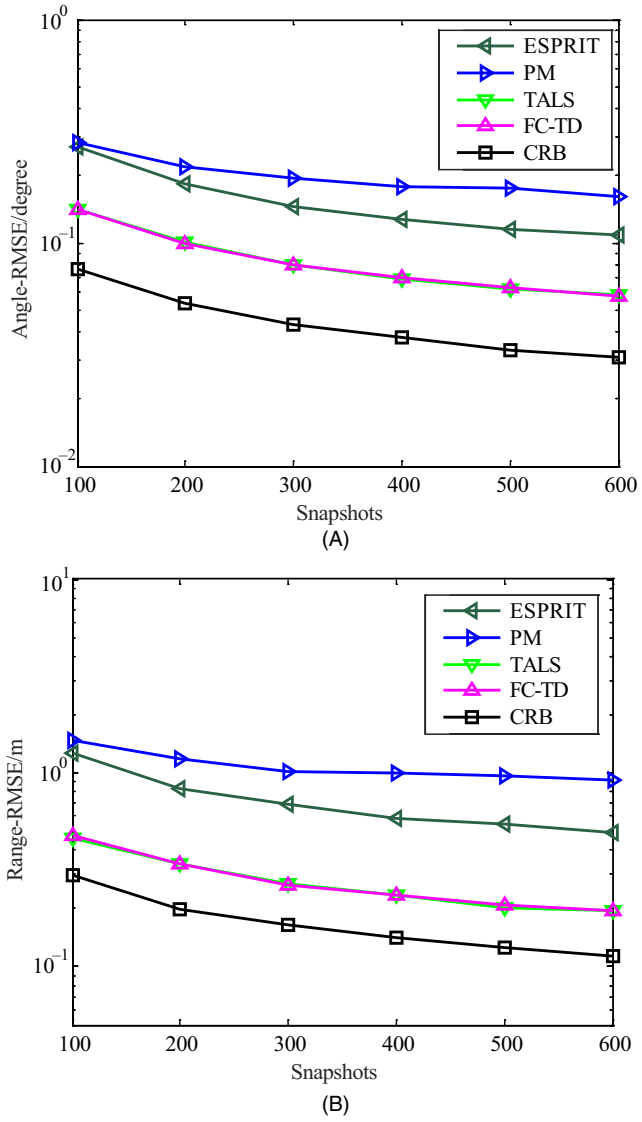

FIGURE 7 (A) Angle RMSE of different algorithms vs snapshots, (B) Range RMSE of different algorithms vs snapshots ($N = 6$, $M = 8$, $K = 3$, $P = 200$, SNR = 5 dB)

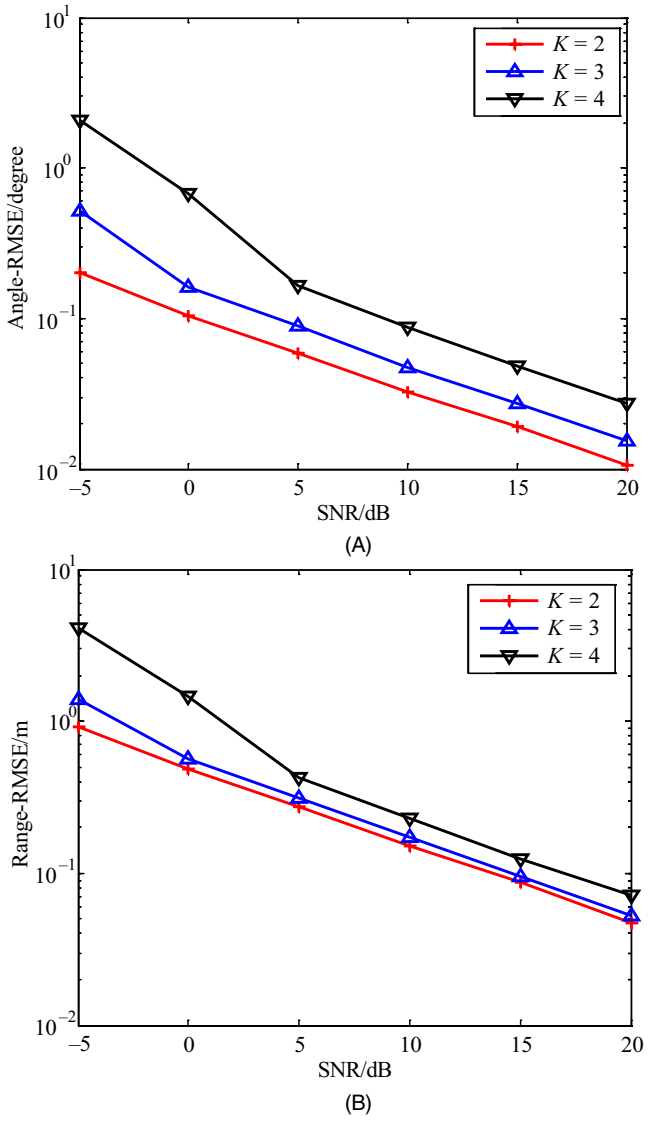

FIGURE 8 (A) Angle RMSE of different K vs SNR, (B) Range RMSE of different K vs SNR ($N = 6$, $M = 8$, $L = 200$, $P = 200$)

used. All results are calculated by $P = 600$ Monte Carlo trials. Particularly, the proposed FC-TD algorithm is compared with the traditional TALS and PM algorithms. The ESPRIT algorithm and CRB are also involved.

Figure 6 depicts the angle and range estimation performance with respect to SNR, respectively, where 200 snapshots are employed for each trial. In Figure 7, the angle and range detection performance vs the number of snapshots is considered, where SNR is set to 5 dB. It is clear that the angle and range estimation performance of all algorithms is improved with the increase of SNR and the number of snapshots. Moreover, the proposed FC-TD algorithm outperforms the PM and ESPRIT algorithms in terms of estimation accuracy. Note that the curves of the traditional TALS algorithm and proposed FC-TD algorithm are overlapped, proving that the proposed FC-TD algorithm can decrease computational complexity but with an estimation performance degradation.

In Figure 8, the angle and range estimation performance of the proposed FC-TD algorithm with different numbers of targets against SNR is given, where $N = 6$, $M = 8$, $L = 200$, and $P = 600$ Monte Carlo trials are conducted for simulation. It is shown that the angle and range estimation performance degrades with an increased number of targets.

Figure 9 plots the angle and range estimation performance of the proposed FC-TD algorithm vs different transmitter element numbers, where $M = 6$, $L = 300$, target 1, and target 2 are detected. To this end, we carry out $P = 600$ Monte Carlo trials. The angle and range estimation

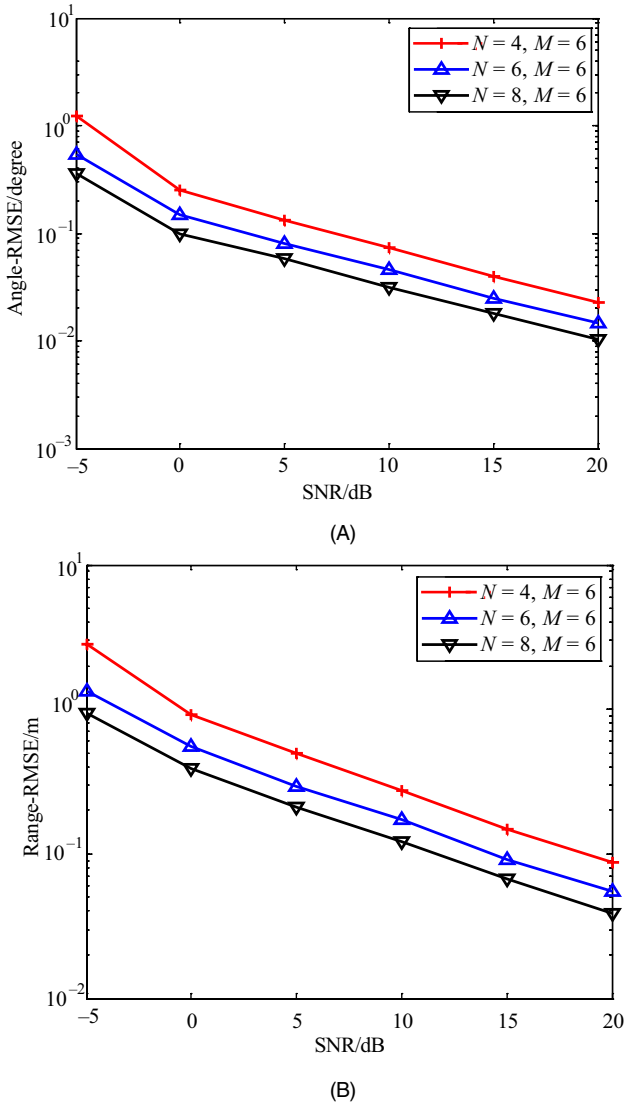

FIGURE 9 (A) Angle RMSE of different N vs SNR, (B) Range RMSE of different N vs SNR ($M = 6$, $K = 2$, $L = 300$, $P = 600$)

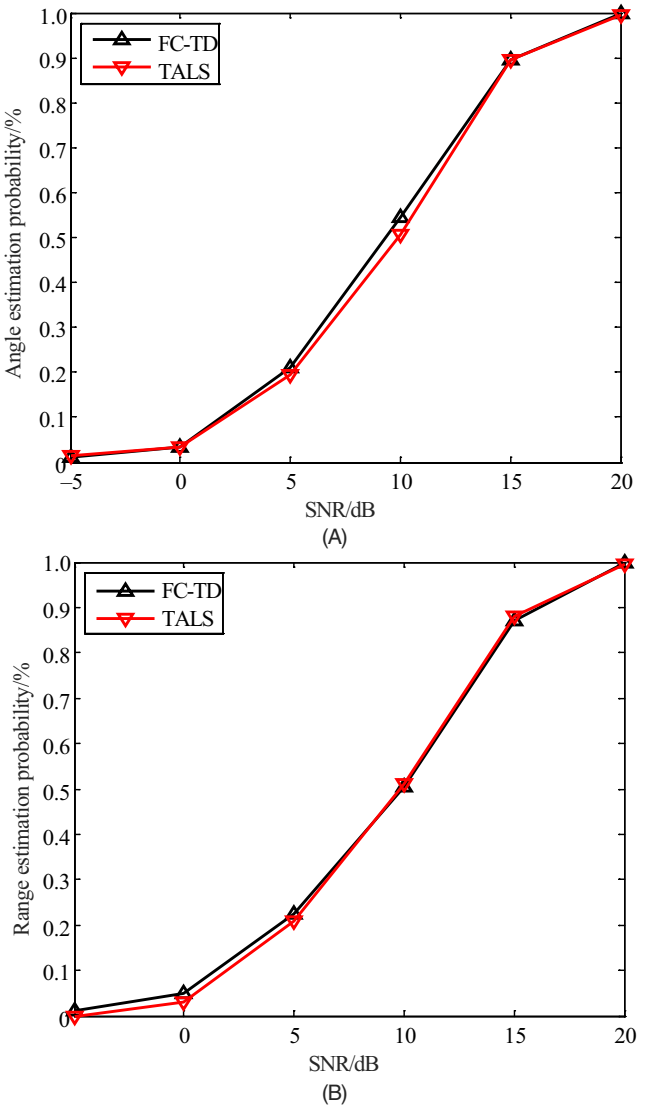

FIGURE 10 (A) Angle resolution vs SNR, (B) Range resolution vs SNR ($N = 6$, $M = 8$, $K = 2$, $L = 200$, $P = 200$)

performance of the proposed FC-TD algorithm improves with the increase of N, which benefits from antenna diversity gain.

In this simulation, the parameter estimation performance of the closely spaced targets is shown. Assume there are two targets need that to be detected and the estimates of the two targets are defined as $(\hat{\theta}_4, \hat{r}_4)$ and $(\hat{\theta}_5, \hat{r}_5)$. The two targets can be detected if $\left|\theta - \hat{\theta}\right| < \left|\theta_4 - \theta_5\right|/2$ and $\left|r - \hat{r}\right| < \left|r_4 - r_5\right|/2$. To investigate the estimation probability of the proposed algorithm, we select two targets of $(\theta_4, r_4) = (20, 200)$ and $(\theta_5, r_5) = (21, 202)$. Figure 10 shows the estimation probability of the proposed FC-TD algorithm and the conventional TALS algorithm vs SNR. It is clear that the proposed FC-TD algorithm has almost the same resolution performance as the conventional TALS algorithm, and they all improve with increased SNR.

6 | CONCLUSION

In this study, we propose an FC-TD algorithm for joint angle and range estimation in the monostatic FDA-MIMO radar. The problem of joint angle and range estimation is first linked to a trilinear model and the traditional TALS algorithm. To reduce excessive iterations and accelerate convergence, the random initialization is replaced by the coarse estimates generated by PM. As a result, the computational complexity of the traditional TALS algorithm is remarkably reduced with no performance degradation. In addition, the coupling information of angle and range is decomposed, and the angle and range estimates are automatically paired. Furthermore, the CRBs of angle and range are provided and the effectiveness of the proposed FC-TD algorithm is validated by numerical simulations.

ACKNOWLEDGMENTS

This work is supported by China NSF Grants (61601167,61971217,61631020), the fund of Sonar Technology Key Laboratory (Research on the theory and algorithm of signal processing for two-dimensional underwater acoustics coprime array, Range estimation and location technology of passive target via multiple array combination) and the Fundamental Research Funds for the Central Universities (NT2019013).

CONFLICT OF INTEREST

The authors declare that there is no conflict of interest regarding the publication of this paper.

ORCID

Cheng Wang https://orcid.org/0000-0001-6639-7256

REFERENCES

1. E. Fishler et al., *MIMO radar: An idea whose time has come*, in Proc. IEEE Radar Conf. (Philadelphia, PA, USA), Apr. 2004, pp. 71–78.
2. J. Li and P. Stoica, *MIMO radar with colocated antennas*, IEEE Signal Process. Mag. **24** (2007), 106–114.
3. I. Bekkerman and J. Tabrikian, *Target detection and localization using MIMO radars and sonars*, IEEE Trans. Signal Process. **54** (2006), 3873–3883.
4. J. Liu, W. Zhou, and F. H. Juwono, *Reweighted smoothed l0-norm based DOA estimation for MIMO radar*, Signal Process. **137** (2017), 44–51.
5. J. Zhang, L. Zhang, and N. Liu, *Maximal likelihood DOA estimation of MIMO radar*, Syst. Eng. Electron. **31** (2009), 1292–1294.
6. R. O. Schmidt, *Multiple emitter location and signal parameter estimation*, IEEE Trans. Antennas Propag. **34** (1986), 276–280.
7. H. Yan, J. Li, and G. Liao, *Multitarget identification and localization using bistatic MIMO radar systems*, EURASIP J. Adv. Signal Process, **2008** (2007), Article no. 283483: 1–8.
8. W. Xia and Z. He, *Multiple-target localization and estimation of MIMO radars using Capon and APES techniques*, in Proc. IEEE Radar Conf. (Rome, Italy), May 2008, pp. 1–6.
9. X. Zhang and D. Xu, *Angle estimation in MIMO radar using reduced-dimension Capon*, Electron. Lett. **46** (2010), 860–861.
10. X. Zhang and D. Xu, *Low-complexity ESPRIT-based DOA estimation for colocated MIMO radar using reduced-dimension transformation*, Electron. Lett. **47** (2011), 283–284.
11. S. Marcos and M. Benidir, *Source bearing estimation and sensor positioning with the propagator method*, in Proc. Annu. Int. Techn. SYmp. Opt. Optoelecotron. Appi. Sci. Eng. (San Diego, CA, USA) 1990, pp. 312–323.
12. D. Nion and N. D. Sidiropoulos, *A PARAFAC based technique for detection and localization of multiple targets in a MIMO radar system*, in Proc. IEEE Int. Conf. Acoustics Speech Signal Process. (Taipei, Taiwan), Apr. 2009, pp. 2077–2080.
13. J. F. Li and D. F. Jiang, *Low-complexity propagator based two dimensional angle estimation for coprime MIMO radar*, IEEE Access. **6** (2018), 13931–13938.
14. R. Z. Cao, X. F. Zhang, and W. Y. Chen, *Compressed sensing parallel factor analysis-based joint angle and doppler frequency estimation for monostatic multiple input multiple output radar*, IET Rad. Sonar Nav. **8** (2014), 597–606.
15. W. Q. Wang, *Range-angle dependent transmit beampattern synthesis for linear frequency diverse arrays*, IEEE Trans. Antennas Propag. **61** (2013), 4073–4081.
16. B. B. Li, W. X. Bai, and G. M. Zheng, *Successive ESPRIT algorithm for joint doa-range-polarization estimation with polarization sensitive FDA-MIMO radar*, IEEE Access **6** (2018), 36376–36382.
17. W. Q. Wang and H. C. So, *Transmit subaperturing for range and angle estimation in frequency diverse array radar*, IEEE Trans. Signal Process. **62** (2014), 2000–2011.
18. X. F. Zhang et al., *Direction of departure (DOD) and direction of arrival (DOA) estimation in MIMO radar with reduced-dimension MUSIC*, IEEE Commun. Lett. **12** (2010), 1161–1163.
19. J. W. Xu et al., *Joint range and angle estimation using MIMO radar with frequency diverse array*, IEEE Trans. Signal Process. **63** (2015), 3396–3410.
20. P. F. Sammartino, C. J. Baker, and H. D. Griffiths, *Frequency diverse MIMO techniques for radar*, IEEE Trans. Aerosp. Electron. Syst. **49** (2013), 201–222.
21. C. D. Meyer, *Matrix analysis and applied linear algebra*, SIAM, Philadelphia, PA, USA, 2000.
22. S. Ahmed, *Product-based pulse integration to combat noise jamming*, IEEE Trans. Aerosp. Electron. Syst. **50** (2014), 2109–2115.
23. J. F. Li and M. Zhou, *Improved trilinear decomposition-based method for angle estimation in multiple-input multiple-output radar*, IET Radar Sonar and Navigat. **7** (2013), 1019–1026.
24. L. Xu et al., *Joint two-dimensional DOA and frequency estimation for L-shaped array via compressed sensing PARAFAC method*, IEEE Access **6** (2018), 34204–37213.
25. L. Y. Xu, F. Q. Wen, and X. F. Zhang, *A novel unitary PARAFAC algorithm for joint DOA and frequency estimation*, IEEE Commun. Lett. **23** (2019), 660–663.
26. N. J. Ruan et al., *A PARAFAC decomposition algorithm for DOA estimation in colocated MIMO radar with imperfect waveforms*, IEEE Access **7** (2019), 14680–14688.
27. J. F. Li, and D. F. Jiang, *Low-complexity propagator based two dimensional angle estimation for coprime MIMO radar*, IEEE Access **6** (2018), 13931–13938.
28. J. F. Li, X. F. Zhang, and C. Han, *Improved two-dimensional DOA estimation algorithm for two-parallel uniform linear arrays using propagator method*, Signal Process. **92** (2012), 3032–3038.
29. P. Gong, X. F. Zhang, and H. Zhai, *DOA estimation for generalized three dimensional coprime arrays: A fast-convergence quadrilinear decomposition algorithm*, IEEE Access **6** (2018), 62419–62431.
30. Q. L. Chen, X. F. Zhang, and R. Z. Cao, *Fast parallel factor decomposition technique for coherently distributed source localization*, J. Syst. Eng. Electron. **29** (2018), 667–675.
31. J. B. Kruskal, *Three-way arrays: Rank and uniqueness of trilinear decompositions, with application to arithmetic complexity and statistics*, Linear Algebra Appl. **18** (1977), 95–138.
32. Z. Zhang et al., *Decoupled 2D direction of arrival estimation in L-shaped array*, IEEE Commun. Lett. **21** (2017), 1989–1992.
33. C. Zhang, H. Huang, and B. Liao, *Direction finding in MIMO radar with unknown mutual coupling*, IEEE Access **5** (2017), 4439–4447.
34. A. Di, *Multiple source location: A matrix decomposition approach*, IEEE Trans. Acoust. Speech Signal Process. **33** (1985), 1086–1091.

35. X. Jie, W. Q. Wang, and K. D. Gao, *FDA-MIMO radar range angle estimation: CRLB, MSE, and resolution analysis*, IEEE Trans. Aerosp. Electron. Syst. **54** (2018), 284–294.

AUTHOR BIOGRAPHIES

Cheng Wang received his BE degree in communication engineering from the College of Information Engineering, West Anhui University, Lu'an, Anhui, China, in 2013, and his ME degree in circuits and systems from the College of Electrical Engineering, Anhui University of Science and Technology, Huainan, Anhui, China, in 2016. He is currently pursuing his PhD degree in communication and information systems from the College of Electronic and Information Engineering, Nanjing University of Aeronautics and Astronautics, Nanjing, Jiangsu, China. His research interests include direction of arrival estimation, array signal processing, and radar signal processing.

Wang Zheng received his BE degree in communication engineering from the College of Electronic and Information Engineering, Nanjing University of Aeronautics and Astronautics, Nanjing, Jiangsu, China, in 2015. He is currently pursuing his PhD degree in communication and information systems from the College of Electronic and Information Engineering, Nanjing University of Aeronautics and Astronautics, Nanjing, Jiangsu, China. His current research interests include array signal processing.

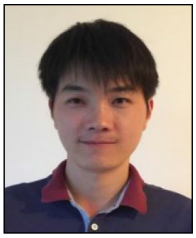

Jianfeng Li received his BE degree in electronic information science and technology from the College of Electronic and Information Engineering, Nanjing University of Aeronautics and Astronautics, Nanjing, Jiangsu, China, in 2010, and his PhD degree in communication and information systems from the College of Electronic and Information Engineering, Nanjing University of Aeronautics and Astronautics, Nanjing, Jiangsu, China, in 2015, where he is now an associate professor. His research interests include array signal processing, parameter estimation, and communication systems.

Pan Gong received her ME degree in communication engineering from Yunnan Minzu University, Kunming, Yunnan, China, in 2016. She is currently pursuing her PhD degree in communication and information systems from the College of Electronic and Information Engineering, Nanjing University of Aeronautics and Astronautics, Nanjing, Jiangsu, China. Her research interests include array signal processing and communication signal processing.

Zheng Li received his ME degree form Qufu Normal University, Qufu, Shandong, China, in 2016. He is currently pursuing his PhD degree in communication and information systems from the College of Electronic and Information Engineering, Nanjing University of Aeronautics and Astronautics, Nanjing, Jiangsu, China. His research interests include array signal processing and direction of arrival estimation